GSA Data Repository 2018017

Depressurization and boiling of a single magmatic fluid as a mechanism for tin-tungsten deposit formation

By Maximilian Korges, Philipp Weis, Volker Lüders and Oscar Laurent

Appendix DR1

GEOLOGICAL BACKGROUND

The Zinnwald granite is hosted by the Teplice rhyolite and has an elliptical shape of ca. 1.4 km x 0.3 km at the surface (Fig. DR1) (Monecke et al., 2007). The granite widens at depth with dips between 20° and 70°. Drill cores document a minimum depth of 1.6 km (Štemprok, 1965, 1971; Štemprok and Sulcek, 1969), but the exact vertical extent of the pluton is unknown.

The Zinnwald granite intruded into the Altenberg-Teplice caldera (Štemprok et al., 2014), which forms the predominant structure of the eastern Erzgebirge magmatic complex. The Caldera was formed by two extrusive events at 326.8 ± 4.3 and 308.8 ± 4.9 Ma, represented by different ignimbrites (Hoffmann et al., 2013) .The Zinnwald/Cínovec granite intruded the Teplice rhyolite between 312.6 ± 2.1 and 314.9 ± 2.3 Ma (Seifert et al., 2011) . However, the dating of granites in the eastern Erzgebirge remains problematic due to their high hydrothermal overprint (Gerstenberger, 1989; Štemprok et al., 2014). Geochemically, it has been interpreted as a highly fractionated A-type (Breiter et al., 1999; Breiter and Škoda, 2012; Sebastian, 2013) similar to the granites at Altenberg and Sadisdorf, which are all characterized by a subvolcanic setting with distinct hydraulic fracturing (Breiter, 2012; Seltmann, 1994). However, the formation of enriched Sn-granites capable of forming economic deposits may require assimilation of pre-concentrated sedimentary rocks during melting (Romer and Kroner, 2015; Romer and Kroner, 2016). The Zinnwald granite itself is

internally complex and can be divided into three different textural types with increasing depth: 1) fine-grained lepidolite-albite granite at the top (Cochrerie et al., 1991; Štemprok and Sulcek, 1969); 2) medium-grained zinnwaldite-albite granite (Johan and Johan, 2004; Rub et al., 1998) with irregular bodies of fine-grained porphyritic zinnwaldite microgranite; 3) porphyritic medium-grained protolithionite granite, which is the main unit of the Zinnwald granite (Johan et al., 2012; Rub et al., 1998).

Sn mineralization mainly occurs in greisen bodies at the endo-contact (Fig. DR1) in the lepidolite-albite granite, which is an equigranular, whitish rock with quartz, albite, potassic feldspar, mica and accessory minerals such as topaz and fluorite (Monecke et al., 2007). The greisen ore bodies have irregular shapes from vertical pipes to horizontal lying bodies, and consist mainly of quartz, mica and topaz (Monecke et al., 2007). Greisenized zones can also be traced to deeper parts of the granite but become less frequent with increasing depth (Neßler et al., 2011; Webster et al., 2004). They can be associated with flat-lying veins but also occur as independent bodies with thicknesses of several tens of meters (Webster et al., 2004).

In contrast to the central greisen-dominated zone, the German part at the northern flank of the mineralized granite is dominated by flat-lying quartz veins ("Flöze") and sub-vertical veins ("Morgengänge"), which contain considerable amounts of wolframite besides cassiterite.

The veins predominantly occur in the upper part of the granite (to 220m depth) and can extend into the Rhyolite (Monecke et al., 2007). Both types (Morgengänge and Flöze) mainly consist of quartz, zinnwaldite and topaz. The horizontal veins are on average 20 to 50 cm thick, but can locally be up to 4 m. The vertical veins are thinner with thicknesses between 10 and 20 cm, but their general mineralogical composition is the same. They trend in NE-SW direction and are formed (or at least reactivated) simultaneously to the horizontal ones (Monecke et al., 2007).

Sn and W from the horizontal and vertical veins have both been historically mined as the main ore at the German part of the mine (which we refer to as the Zinnwald deposit in this paper, because the Czech part is called Cínovec). The predominance of the high ore grades within the horizontal veins is documented by the orientation and naming of the historical mining tunnels which basically followed their extent (Fig. DR1). The mineralization is localized and heterogeneous, with high grade parts next to barren quartz veins. Greisen bodies around the veins have mostly limited dimensions of a few cm to several m and are more irregular in their spatial expansion in comparison to the independent greisen bodies (Fig.

DR2). The relationship of joints and mineralized veins in the Zinnwald granite is still discussed. We briefly summarize the main aspects here and the reader is referred to Štemprok et al. (1994) and Breiter et al. (2017) for further details.

The flat-lying veins in Zinnwald dip into NE direction and are subparallel to the granite-rhyolith surface. They are occurring together with greisen bodies for which, in the southern part, a relation to irregular steep joints has been reported (Breiter et al., 2017). This joint system is explained by hydraulic fracturing due to fluid exsolution from the crystallizing magma chamber. However, in the norther part the influence of steep fluid pathways is limited and the veins and greisens are related to more flat-lying joints (Breiter et al., 2017), which are indicative for a formation under near lithostatic pressure. At Panasqueira, the formation of sub-horizontal veins has been attributed to episodic pressure decreases during vein formation due to hydraulic valving (cycles of fluid injection) (Foxford et al., 2000). Episodic injection of fluid may also be documented in the Zinnwald veins by growth zones around coarse grained quartz (Bons et al., 2012) and multiple fluid pulses have been inferred by Breiter et al. (2017). Further, the heterogeneous distribution of the ore could be indication for dynamic fluid pulses.

Some parts of the horizontal veins show a high amount of zinnwaldite at their selvages and these occurrences are currently explored as a possible Li resource (Neßler et al., 2011; Neßler et al., 2014). There are a few analyses of fluid inclusions in Zinnwald but with less focus in the detailed precipitation mechanism itself (Durisova et al., 1979; Graupner et al., 2005; Thomas, 1982; Thomas and Baumann, 1980). The fluid evolution and the relative timing of formation of greisen, veins and ores remain unclear.

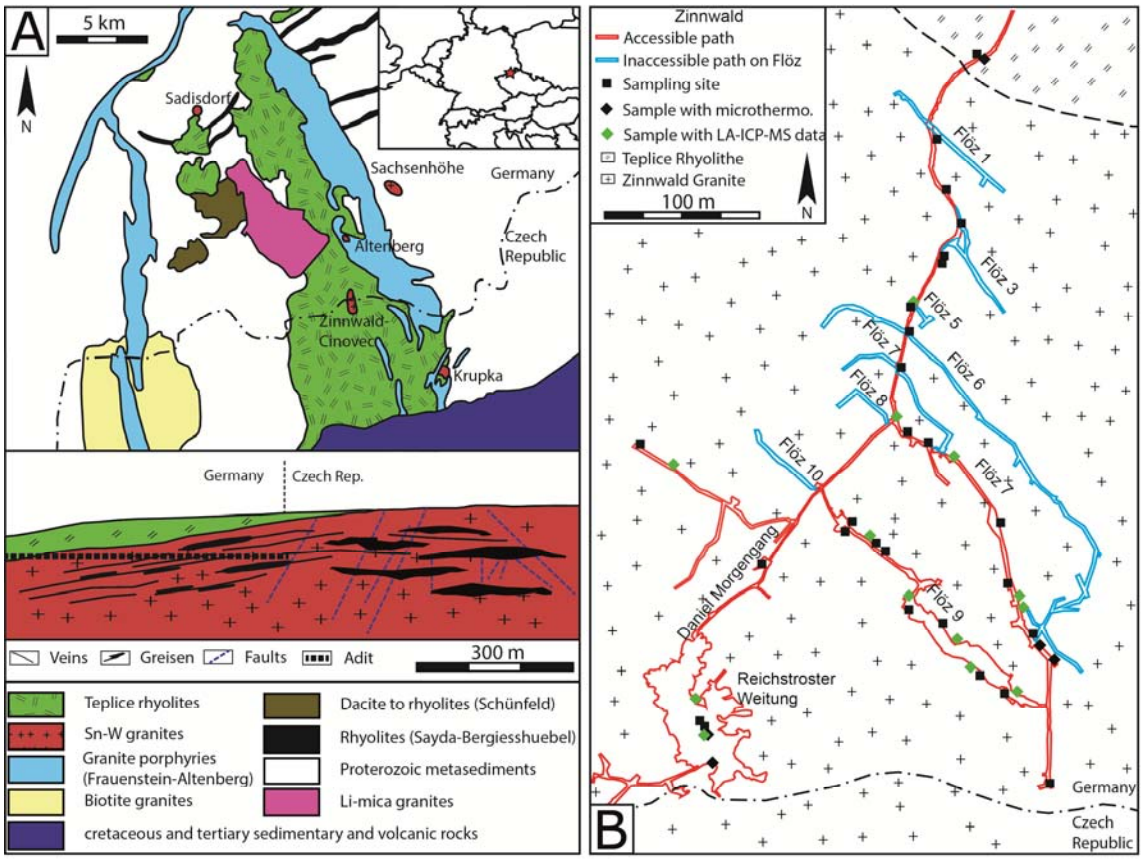

Figure DR1. A: Geological map of the Zinnwald area (after Dolejš and Štemprok (2001) with schematic geological cross section through the granite cupola (after Štemprok et al. (1994), the sampling area "Tiefer Bünau Stollen" (adit entrance: 5413041(E) 5623549(N)) is located in the German part of the deposit. B: Sampling points in the adit along the accessible parts of the formerly mined veins (Flöze). Symbols indicate the different used analytical techniques.

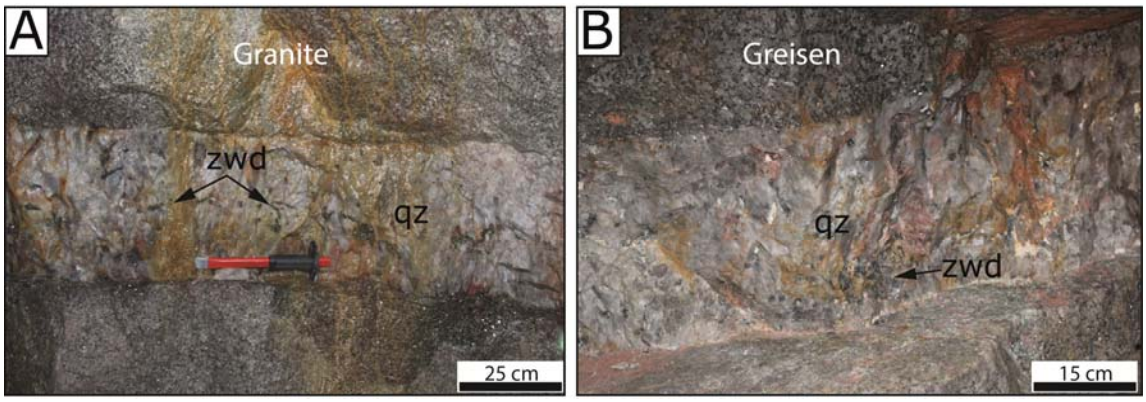

Figure DR2. Flöz 9 quartz (qz) vein with zinnwaldite (zwd) in contact with granite (A) and greisen (B).

SAMPLE ORIGIN

The Zinnwald deposit is partially accessible, because of its use as a historical visitors mine and for Li exploration. We systematically sampled the horizontal and vertical quartz veins being exposed in the deposit (Fig. DR1). The vein quartz shows highly variable (often chevron) textures, ranging from clear to milky with signs for recrystallization. The sample suite from the mine comprises a total of 50 quartz samples, from which 17 were used for microthermometry and a subset of 13 for chemical analyses with LA-ICPMS.

Ore specimens are almost absent in the remaining underground exposures because of the extensive past mining activities. Therefore, we obtained additional 28 samples containing crystals of cassiterite, wolframite and quartz from mineral collections of the Federal Institute for Geosciences and Natural Resources (BGR), the Museum für Naturkunde Berlin and the ETH Zurich. The old labels and sample descriptions are not detailed enough to perfectly locate the samples, but all labels related to Zinnwald, Sachsen (Saxony), can most likely be attributed to the German part of the mine.

A subset of eight samples was used for microthermometry and LA-ICPMS (Tab. A1), providing data from wolframite, cassiterite and quartz. One vein sample included intergrown cassiterite and wolframite together with quartz (ZWD B9), showing coeval precipitation of the two ore minerals. Other crystals from vein samples included pure wolframite or wolframite intergrown with quartz. A further sample contains vein-hosted cassiterite with quartz (HU8). One greisen sample (HU 4) contains small quartz grains intergrown with cassiterite of reddish to brown color. We further analyzed quartz crystals from the BGR archive (ZWD B12) and re-analyzed a euhedral crystal from ETH Zurich (Zinw 1) (Heinrich et al., 1999).

TABLE A1. SAMPLES OF ORE AND GANGUE MINERALS FROM COLLECTIONS.

Collection	Mineral	Sample number	Type	Measured FI in
BGR	Qz	ZWD B2	Vein	Qz
BGR	Qz, Wf	ZWD B5	Vein	Wf
BGR	Qz, Wf, Cst	ZWD B9	Vein	Wf, Cst
BGR	Wf	ZWD B10	Vein	Wf
BGR	Qz	ZWD B12	Vein	Qz
Museum für Naturkunde Berlin	Qz, Cst	HU 4	Greisen	Qz, Cst
Museum für Naturkunde Berlin	Qz, Cst	HU 8	Vein	Qz,Cst
ETH Zurich	Qz	Zinw 1	Vein	Qz

METHODS

Fluid inclusions in quartz were studied in transmitted light using a FLUID INC. adapted USGS heating/freezing stage with an Olympus BX 50 microscope. Fluid inclusions hosted in wolframite were analyzed with a Linkham THMS 600 system with an Olympus BHSM-IR microscope. The infrared image is transmitted to a monitor by a QCam-IR camera. For calibration, synthetic fluid inclusions standards by Synflinc were used. Cassiterite showed varying transmittance and was therefore studied in transmitted light and near-infrared light. However, IR and transmitted light always revealed the same homogenization and ice melting temperatures. As CO_2 concentrations are generally very low, pressure estimates were calculated using the phase relations of the H_2O-NaCl system as described in Driesner and Heinrich (2007) and Driesner (2007).

LA-ICP-MS measurements were performed at ETH Zurich using a GeoLas system (LambaPhysik-Coherent, Germany) equipped with a 193 nm ArF-Excimer laser ablation system coupled to a Perkin Elmer Elan 6100 DRC quadrupole IC mass spectrometer for multi-element analysis (see Günther et al. (1998)for a detailed description). The samples were analyzed either in a ca. 1 cm^3 rhomb-shaped, stainless steel cell (cassiterite- and wolframite-hosted inclusions); or a ca. 5 cm^3 round glass cell (quartz-hosted inclusions). The cell was fluxed with carrier gas consisting of high-purity (5.0 grade) He (1.1 L.min–1), to which H2 was added (5 mL.min–1) to enhance sensitivity for heavy elements (Guillong and Heinrich, 2007). Sample gas consisting of 6.0 grade Ar (ca. 0.8 L.min–1) was admixed downstream of the ablation cell prior to injection in the plasma. The ICP-MS was tuned for maximum sensitivity and low oxide rate formation (248ThO+/232Th+ <1%). The glass standard NIST SRM 610 was used as the primary reference material (using conventional standard bracketing) and analyzed with 40 μm pit size, repetition rates of 10 Hz and ca. 1 min measurement consisting of 30 s gas blank + 30 s ablation. FI in quartz were analyzed by slowly incrementing the spot size using an opening aperture (Gagnon et al., 2003). Depending on the behavior of the host quartz, repetition rates of 10 or 20 Hz with laser output energies between 110 and 170 mJ (corresponding to energy densities on sample of ca. 14 to 18 J.cm–2) were applied. Cassiterite and wolframite were analyzed with a repetition rate of 10 Hz and output energies of 40 – 60 mJ (energy densities of ca. 5 to 7 J.cm–2). Fluid inclusions in wolframite could not be relocated directly with the given LA-ICP-MS setup and were therefore retrieved via a documentation of IR, coupled IR and reflected light, and reflected light photomicrographs. In total, we measured 25 elements (7Li, 11B, 23Na, 39K, 55Mn, 57Fe, 65Cu, 66Zn, 75As , 85Rb, 97Mo, 118Sn, 133Cs, 182W, 208Pb, 88Sr, 29Si, 43Ca, 93Nb, 107Ag, 121Sb, 181Ta, 197Au, 238U, 209Bi) and subsequently reduced the data with

157 the SILLS software (Guillong et al., 2008),using the salinity (wt.% eq. NaCl) determined by
158 microthermometry as internal standard.
159 Despite the small amount of CO_2 stable carbon isotopic compositions in fluid
160 inclusions could be measured using a sample crusher connected via a gas chromatography
161 column to an elemental analyzer isotope ratio mass spectrometry system. This analytical setup
162 allows online simultaneous measurements of stable isotope ratios of N_2, CH_4, and CO_2 in
163 natural gas mixtures released by crushing of fluid inclusions. For details see Lüders et al.
164 (2012) and Plessen and Lüders (2012).
165
166 **ADDITIONAL FLUID INCLUSIONS DATA**
167
168 We classified primary and pesudosecondary fluid inclusions and fluid inclusion
169 assemblages (FIAs) according to definitions by Goldstein (2003) and Roedder (1984). A FIA
170 describes a group of fluid inclusions (FIs) which were entrapped at the same time. Due to the
171 appearance of primary and pseudosecondary FIs, they can be directly related to crystal
172 growth. Primary inclusions are typically entrapped along growth zones and are caused by
173 small irregularities during the formation of the crystal. Pseudosecondary FIs are entrapped
174 before the formation of the crystal is finished (Goldstein, 2003) by healing of microfractures,
175 followed by further crystal growth. The different FI types were grouped by their appearance,
176 homogenization temperature and salinity (Tab. A2). The type numbering is based on
177 decreasing homogenization temperatures. However, there is no petrographic evidence that this
178 ordering reflects a sequence in space and/or time.
179
180 **Fluid inclusions types**
181 ***Type I***
182 This type of inclusion was mainly detectable in one quartz crystal probably from the
183 central part of the deposit (Zinw 1). It contains boiling assemblages which are arranged along
184 large trails together with vapor inclusions. Type I FIs were also observed in a distinct area of
185 another sample of the BGR collection (ZWD B12).
186
187 ***Type II***
188 Type IIa inclusions in greisen cassiterite were mostly arranged in groups of two or
189 three inclusions in a growth zone, with sizes between 10 and 40 μm. The FIs have salinities
190 between 5 and 8 wt.% NaCl equiv. and show homogenization temperatures in the range
191 between 350 and 390°C. The FIA in the adjacent small quartz crystal appear as clusters with
192 mostly elongated shapes and sizes of up to 50 μm (Fig. DR3). FIs in quartz are also type IIa

inclusions. However, some FIs preferably homogenize into the vapor phase with slightly higher Th of 400°C. The FIs in greisen (type IIa) are similar to those of the quartz veins (type IIb)

Type IIb are the most common primary FI in vein quartz and decorate growth zones or occur in rare FIA (Fig. DR3). FI sizes normally range between 10 and 20 μm, but some exceptional big FI up to 50 μm were observed in the center of growth zones. Homogenization temperatures vary within a relatively small range between 350°C and 410°C with the majority between 370 and 380 °C. Salinities show a broad range from 1 to 8.5 wt.% NaCl equiv. The results are similar to temperatures and salinities from earlier fluid inclusion studies (Thomas, 1982).

Type III

IR-microscopy revealed that the studied wolframite samples are crosscut by numerous cracks and that part of the crystals are even opaque under IR light. However, other parts of the samples exhibit primary growth zones with type IIIa inclusions with sizes from <5 up to 40 μm. Locally, liquid-rich FIs occur together with small vapor-rich inclusions which could not be measured. However, the presence of co-existing liquid and vapor-rich FIA are evidence for boiling of the ore-forming fluid (ZWD B5, Fig. DR3). Therefore, the liquid-rich type III inclusions represent the brine end-member of the boiling assemblage. The wolframite samples contain later quartz in fissures but also earlier quartz crystals (ZWD B2) which have been overgrown by the wolframite. This earlier quartz contains some measurable fluid inclusions of small size (max 10 μm) which can be classified by their appearance, salinity and Th as type II inclusions (Fig. DR3). Both cassiterites from vein samples (ZWD B9, HU 8) show highly variable transparency (Fig. DR3) and fluid inclusion data were obtained mainly by IR microthermometry. Type IIIb FIs in vein cassiterite are aqueous 2-phase with sizes of up to 40 μm.

Type IV

Type IV FIAs were detectable in Flöz 9 consisting of brine- and vapor-rich inclusions. Due to their small amount of liquid, no phase transitions in coexisting vapor-rich inclusions could be measured. Flöz 9 also contains type IIb inclusions, but the petrographic relationship between the two inclusion types is not documented.

Type V (secondary)

227 Type V FIs are the most frequent in all samples from the quartz veins (Fig.3). The
228 majority of them have small sizes of less than 5 μm and occur in clouds or are arranged along
229 large trails crosscutting the quartz crystals. Rarely, some clusters with bigger secondary FI
230 with small vapor bubbles and diameters of up to 30 μm were observed that homogenize at
231 temperatures of <=300°C and have salinities of about 2.5 wt.% NaCl equiv. and below. Type
232 V inclusions are only documented in the supplementary material and are omitted in the main
233 text of the paper, because these secondary inclusions likely represent post-ore stages of the
234 system.

235 TABLE A2. OVERVIEW OF THE DIFFERENT FLUID INCLUSIONS TYPES

FI type	T_h (°C)	Salinity (wt% NaCl eq.)	Host rock	Host mineral	Phases (at room temperature)
I	420 - 490	~40	Vein	Qz	Liquid, vapor & salt
IIa	350 - 400	5 - 8	Greisen	Qz, cst	Liquid & vapor
IIb	350 - 410	1 - 9	Vein	Qz	Liquid & vapor
IIIa	340 - 350	10 - 12	Vein	Wf	Liquid & vapor
IIIb	330 - 340	~14	Vein	Cst	Liquid & vapor
IV	290 - 310	~30	Vein	Qz	Liquid, vapor & salt
V	<300	<2.5	Vein	Qz, wf, cst	Liquid & vapor

236

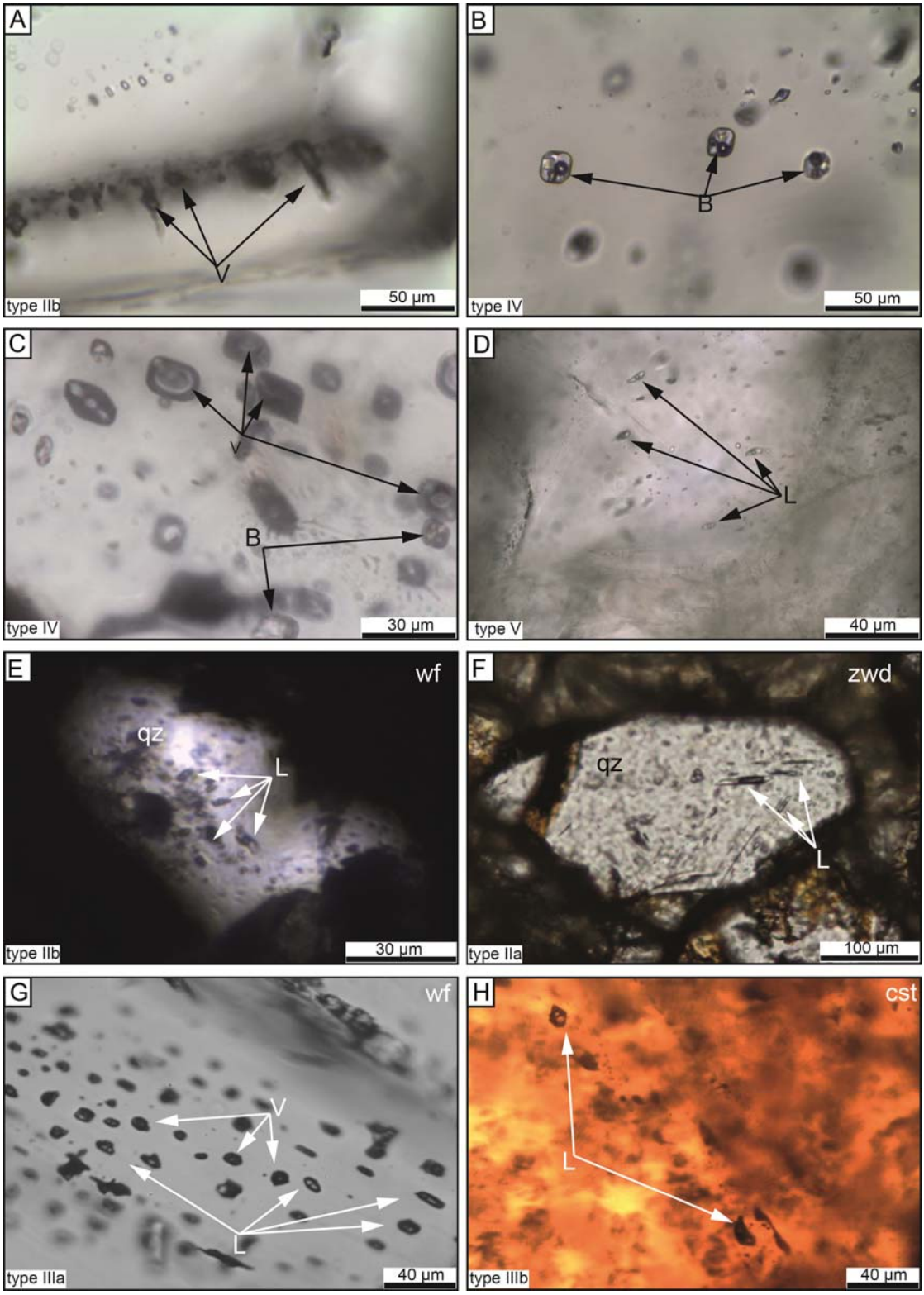

Figure DR3. A: Primary vapor-rich fluid inclusions (V) of type II decorating a growth zone in quartz (ZWD 29). B: Trail of type IV brine-type inclusions (B) in quartz from Flöz 9 (ZWD 14). C: Boiling trail of type IV at a different location of Flöz 9. D: Seconadry low density FI (type V). E: Wolframite with enclosed quartz hosting 2-phase FIs of type II (ZWD B2). F: Single quartz crystal in greisen quartz embedded in zinnwaldite (HU 4) with FI of type II. G: Wolframite (ZWD B10) with a type IIIa

boiling assemblage of co-existing intermediate density liquid-rich inclusions (L) and with vapor-rich inclusions (V). H: Inclusion trail of type III in vein cassiterite (HU 8)

Fluid inclusions composition

Despite their different properties, the chemical data obtained by LA-ICP-MS reveal many similarities between the different FI types. Measurements of Sn concentrations by LA-ICP-MS were difficult due to the high background (Schlöglova et al., 2017). However, Sn could be detected in some type IIb inclusions but was rarely measured in IIa inclusions (Fig. DR4). The Sn content is relatively constant with ca. 380 ppm and maximum values of up to 2900 ppm. The average Sn contents in type I brine inclusions is about 710 ppm and 1500 ppm for type IV FI. Wolframite has higher backgrounds for Sn, but some IIIa FIs have detectable Sn contents of up to 2400 ppm.

The Mn contents in brines of type I and IV are similar with average values of 28000 ppm and 24000 ppm, respectively. Fe concentrations have the same range like Mn in type I (25000 ppm) but lower values in type IV (15000 ppm), whereas the W contents are comparable in both brine generations (176 ppm and 168 ppm). In some type II inclusions, Fe was above the limit of detection (2000 – 10000 ppm,) resulting in contents of up to tens of thousands ppm in some greisen FI and up to 11000 ppm in the quartz veins. The rare FI with measurable W peaks had average contents of 92 ppm in the greisen (IIa) and 105 ppm in the quartz veins (IIb).

The most abundant elements in the FI besides Na are Cs and Rb, which were detected in almost all different inclusion generations independent of the host. Their contents depend on salinity with up to 9000 ppm of Cs and 15 000 ppm of Rb in brine-type inclusions of types I and IV, in contrast to the type IIb inclusions with averages of 170 ppm Cs and 240 ppm Rb. Type IIa and III have higher contents of both elements, due to their slightly higher salinity (300 ppm Rb, 620 ppm Cs in the greisen (IIa) and 2500 ppm Rb, 2000 ppm Cs in ore mineral-hosted type III FI). Pb and Zn show low contents in the type II but are higher in brines-type inclusions of type I and IV.

High saline inclusions of I, IV and III also contain high amounts of K, sometimes with even higher contents than Na, while K contents are lower or below the detection limit in type IIb. The contents of trace elements such as Li, B and As are relatively constant in all different FI generations in quartz (I, II, IV), mainly varying between 300 and 1000 ppm, but are generally higher in FIs hosted in ore minerals (III).

The almost linear relation between some elements shown in the study is further documented by an almost linear positive correlation between Cs and Rb with Cs:Rb ratios

between 1:1 and 1:2. A similar correlation is also given in the Cs:Na plot for type IIa and IIb but not for higher saline FIs of type III, IV and I, showing relatively constant Na contents but varying Cs contents (Fig. DR5). Linear correlation patterns are also visible in other element ratios, e.g. by replacing Cs with K (Fig. DR5). Replacing Rb by Pb (Fig. DR5) suggests that Pb concentrations in type III FI are reduced compared to those in FIs in quartz, which is also visible when plotting As vs. Pb (Fig. DR5). These lower contents can be explained by different compatibilities of Pb in ore minerals in contrast to quartz, which can modify the FI contents after entrapment (James and MacNaughton, 1977).The linear correlation of elements shown in Fig. DR5 between all fluid inclusions types is further confirmed by other elements such as Mn and Zn, which are not particularly related geochemically and support the interpretation of a single source fluid (Fig. DR 5). These trends are independent of the origin of the samples (from the mine or from collections) and are, together with the homogeneous element content within one inclusion type (especially for vein quartz from the mine and the collection) and their similar appearance (L-V-ratio, salinity, homogenization), an important confirmation for the validity of the samples from the mineral collections.

Further, the geochemical data show that fluid inclusions in all type II (both in vein quartz and greisen) have similar element contents (Fig. DR5) whereas the FI from boiling assemblages (type I, III, IV) form a distinct cluster of high element concentrations. The samples in boiling FIA from the archives (type I and III) show the same behavior as the boiling assemblages from Flöz 9 (type IV). This association is also documented by opposing trends in the Na vs. Cs plot, showing a positive correlation at low concentrations in type II inclusions, whereas type I, III and IV inclusions indicate a slight decrease in Cs for the highest Na concentration. These similar trends between the distinct boiling FIAs in the quartz (I, IV) and the FI in the ore (II) are not only visible in the several diagrams, they are also distinct by comparing the medians and means of the elements with each other (see Appendix DR2). Here, the data further proves the same ranges of these different mineralogical generations (summarized in Fig. DR6). This supports the observation that the type III assemblages, consisting of liquid and vapor rich inclusions, represent boiling assemblages. The described relation between type I, III and IV can also be detected in the linear trends but are furthermore visible in additional x-y diagrams. Certain elements seem to undergo an enrichment/depletion process during boiling which is preserved only in those plots.

LA ICP-MS data reveal that there are two trends visible in Fig. DR5: 1) the linear trend supporting the interpretation of a single magmatic fluid and 2) the high amount of

312 overlap between type I, III and IV in contract to the inclusions of II as a second indication for
313 boiling of type III fluid inclusions.
314

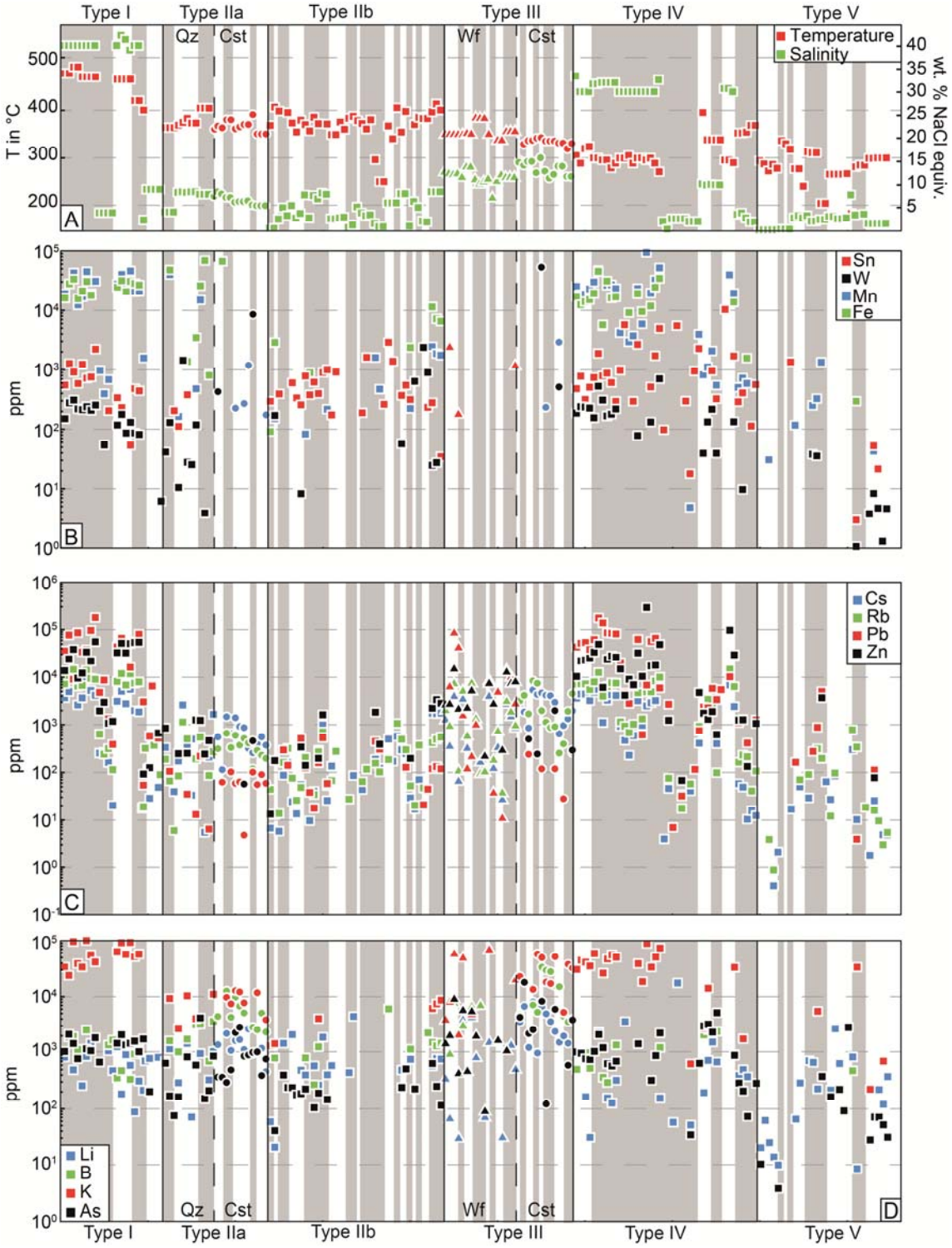

315

316 Figure DR4. A: Homogenization temperature and salinity of fluid inclusions with added secondary
317 inclusions (type V) B-D: Element contents in fluid inclusions hosted in quartz (squares), cassiterite

(circles) and wolframite (triangles) (LA-ICP-MS analyses). Grey and white areas indicate fluid inclusion assemblages. Shapes of the symbols indicate the host mineral.

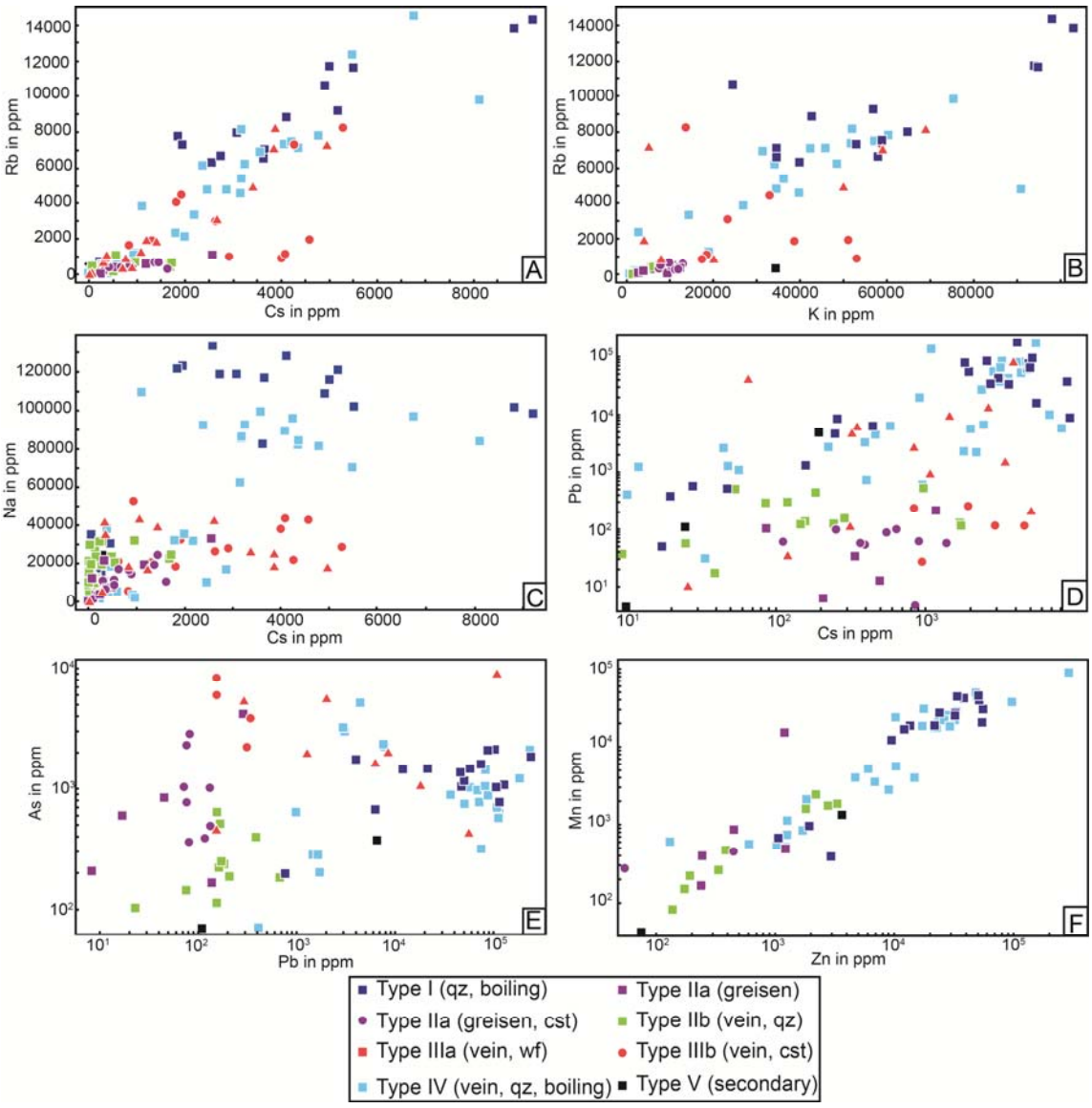

Figure DR5. Chemical variations of Rb vs. Cs (A), Rb vs. K (B), Na vs. Cs (C), Pb vs. Cs (D), As vs. Pb (E) and Mn vs. Zn (F) showing near-linear trends (A, B, F) suggesting a common source fluid as well as an association of type IIa fluids (Greisen quartz and cassiterite) with type IIb fluids from vein quartz and an assocation of type III fluids (Vein wolframite and cassiterite) with brine end-members from boiling assemblages of type I and IV inclusions in vein quartz.

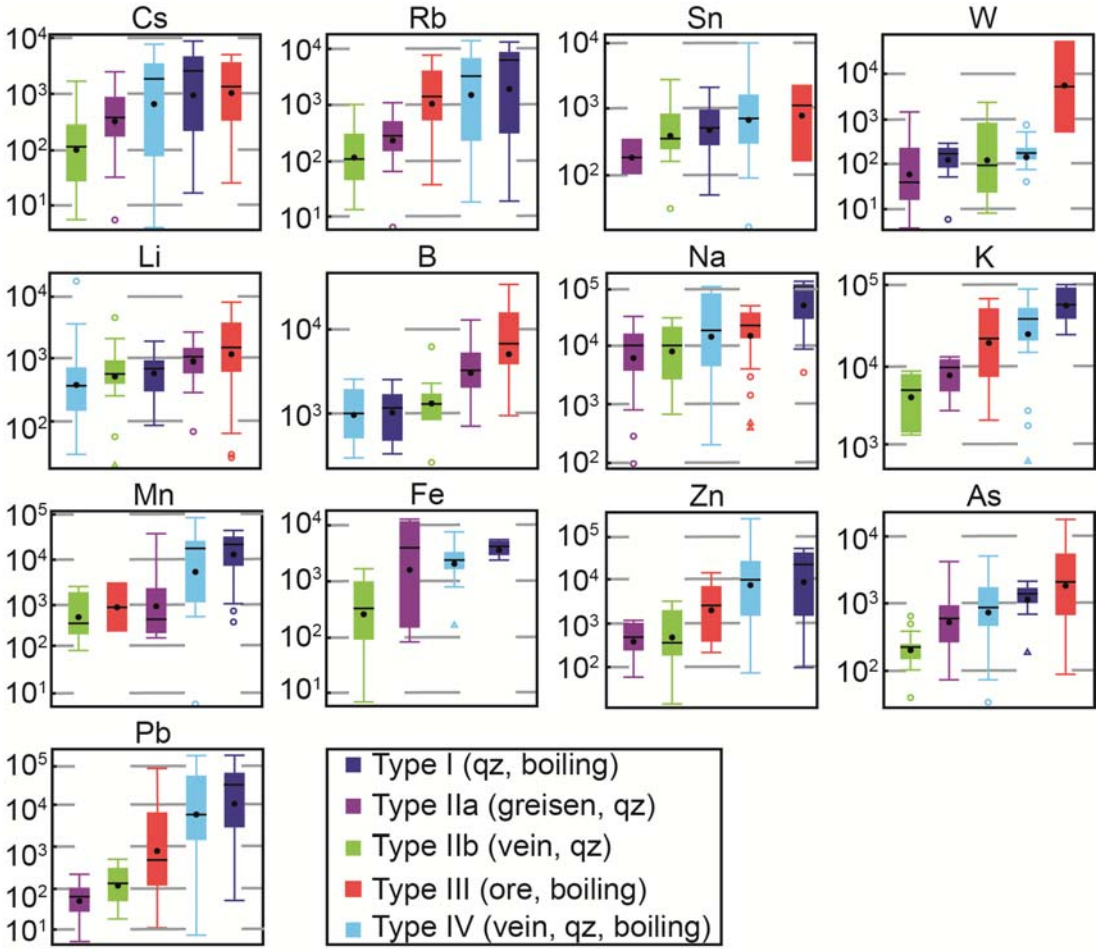

328

329 Figure DR6. Chemical variations of the main elements, sorted after increasing mean values (black
330 circle), showing the similar contents of type III fluids (in red) with brine end-members from boiling
331 assemblages of type I and IV inclusions in quartz (blueish). Black lines refer to the median, the bottom
332 of the boxes represent the first quartile (25% of the data) and the top the third quartile (75% of the
333 data), the whiskers are the extreme values that are not outliners, an outliner (circle) is further than
334 1.5*(Q3-Q1) from the box, a far outliner is futher than 3*(Q3-Q1) from the box.

335

336 Bons, P. D., Elburg, M. A., and Gomez-Rivas, E., 2012, A review of the formation of tectonic veins
337 and their microstructures: Journal of Structural Geology, v. 43, p. 33-62.
338 Breiter, K., 2012, Nearly contemporaneous evolution of the A-and S-type fractionated granites in the
339 Krušné hory/Erzgebirge Mts., Central Europe: Lithos, v. 151, p. 105-121.
340 Breiter, K., Ďurišová, J., Hrstka, T., Korbelová, Z., Vaňková, M., Galiová, M. V., Kanický, V.,
341 Rambousek, P., Knésl, I., and Dobeš, P., 2017, Assessment of magmatic vs. metasomatic
342 processes in rare-metal granites: A case study of the Cínovec/Zinnwald Sn-W-Li deposit,
343 Central Europe: Lithos, v. 292-293, p. 198-217.
344 Breiter, K., Forster, H. J., and Seltmann, R., 1999, Variscan silicic magmatism and related tin-tungsten
345 mineralization in the Erzgebirge-Slavkovsky les metallogenic province: Mineralium Deposita,
346 v. 34, p. 505-521.
347 Breiter, K., and Škoda, R., 2012, Vertical zonality of fractionated granite plutons reflected in zircon
348 chemistry: the Cínovec A-type versus the Beauvoir S-type suite: Geologica Carpathica, v. 63,
349 no. 5, p. 383-398.

Cochrerie, A., Johan, V., Rossi, P., and Štemprok, M., 1991, Trace element variations and lanthanide tetrad effect studied in a Variscan lithium albite granite: case of the Cínovec granite (Czechoslovakia). *in* Pagel, M., and Leroy, J. L., eds., Source, Transport and Deposition of Metals: Rotterdam, p. 745-749.

Dolejš, D., and Štemprok, M., 2001, Magmatic and hydrothermal evolution ofLi-F granites: Cínovec and Krásnointrusions, Krušné hory batholith, Czech Republic: Bulletin of Czech Geological Survey, v. 76, no. 2, p. 77-99.

Driesner, T., 2007, The system H2O–NaCl. Part II: Correlations for molar volume, enthalpy, and isobaric heat capacity from 0 to 1000 °C, 1 to 5000 bar, and 0 to 1 XNaCl: Geochimica et Cosmochimica Acta, v. 71, no. 20, p. 4902-4919.

Driesner, T., and Heinrich, C. A., 2007, The system H2O–NaCl. Part I: Correlation formulae for phase relations in temperature–pressure–composition space from 0 to 1000°C, 0 to 5000bar, and 0 to 1 XNaCl: Geochimica et Cosmochimica Acta, v. 71, no. 20, p. 4880-4901.

Durisova, J., Charoy, B., and Weisbrod, A., 1979, Fluid inclusion studies in minerals from tin and tungsten deposits in the Krusne Hory Mountains (Czechoslovakia): Bulletin de Minéralogie, v. 102, no. 5-6, p. 665-675.

Foxford, K., Nicholson, R., Polya, D., and Hebblethwaite, R., 2000, Extensional failure and hydraulic valving at Minas da Panasqueira, Portugal: evidence from vein spatial distributions, displacements and geometries: Journal of Structural Geology, v. 22, no. 8, p. 1065-1086.

Gagnon, J. E., Samson, I. M., and Fryer, B. J., 2003, LA-ICP-MS Analysis of Fluid Inclusions, *in* Samson, I., Anderson, A., and Marshall, D. D., eds., Fluid Inclusions Analysis and Interpretation, Volume 32: Vancouver, Mineral Associaton of Canada, p. 391-323.

Gerstenberger, H., 1989, Autometasomatic Rb enrichments in highly evolved granites causing lowered RbSr isochron intercepts: Earth and Planetary Science Letters, v. 93, no. 1, p. 65-75.

Goldstein, R. H., 2003, Petrographic Analysis of Fluid Inclusions, *in* Samson, I., Anderson, A., and Marshall, D., eds., Fluid inclusions: Analysis and interpretation, Volume 32: Vancouver, Mineralogical Association of Canada, p. 9-53.

Graupner, T., Brätz, H., and Klemd, R., 2005, LA-ICP-MS micro-analysis of fluid inclusions in quartz using a commercial Merchantek 266 nm Nd: YAG laser: European journal of mineralogy, v. 17, no. 1, p. 93-102.

Guillong, M., and Heinrich, C. A., 2007, Sensitivity enhancement in laser ablation ICP-MS using small amounts of hydrogen in the carrier gas: Journal of Analytical Atomic Spectrometry, v. 22, no. 12, p. 1488-1494.

Guillong, M., Meier, D. L., Allan, M. M., Heinrich, C. A., and Yardley, B. W., 2008, Appendix A6: SILLS: A MATLAB-based program for the reduction of laser ablation ICP-MS data of homogeneous materials and inclusions: Mineralogical Association of Canada Short Course, v. 40, p. 328-333.

Günther, D., Audétat, A., Frischknecht, R., and Heinrich, C. A., 1998, Quantitative analysis of major, minor and trace elements in fluid inclusions using laser ablation–inductively coupled plasmamass spectrometry: Journal of Analytical Atomic Spectrometry, v. 13, no. 4, p. 263-270.

Heinrich, C. A., Günther, D., Audétat, A., Ulrich, T., and Frischknecht, R., 1999, Metal fractionation between magmatic brine and vapor, determined by microanalysis of fluid inclusions: Geology, v. 27, no. 8, p. 755-758.

Hoffmann, U., Breitkreuz, C., Breiter, K., Sergeev, S., Stanek, K., and Tichomirowa, M., 2013, Carboniferous–Permian volcanic evolution in Central Europe—U/Pb ages of volcanic rocks in Saxony (Germany) and northern Bohemia (Czech Republic): International Journal of Earth Sciences, v. 102, no. 1, p. 73-99.

James, R., and MacNaughton, M., 1977, The adsorption of aqueous heavy metals on inorganic minerals: Geochimica et Cosmochimica Acta, v. 41, no. 11, p. 1549-1555.

Johan, Z., and Johan, V., 2004, Accessory minerals of the Cínovec (Zinnwald) granite cupola, Czech Republic: indicators of petrogenetic evolution: Mineralogy and Petrology, v. 83, no. 1-2, p. 113-150.

Johan, Z., Strnad, L., and Johan, V., 2012, Evolution of the Cínovec (zinnwald) Granite Cupola, Czech Republic: Composition of Feldspars and Micas, a Clue to the Origin of W, sn Mineralization: The Canadian Mineralogist, v. 50, no. 4, p. 1131-1148.

Lüders, V., Plessen, B., and di Primio, R., 2012, Stable carbon isotopic ratios of CH 4–CO 2-bearing fluid inclusions in fracture-fill mineralization from the Lower Saxony Basin (Germany)–A tool for tracing gas sources and maturity: Marine and Petroleum Geology, v. 30, no. 1, p. 174-183.

Monecke, T., Dulski, P., and Kempe, U., 2007, Origin of convex tetrads in rare earth element patterns of hydrothermally altered siliceous igneous rocks from the Zinnwald Sn–W deposit, Germany: Geochimica et Cosmochimica Acta, v. 71, no. 2, p. 335-353.

Neßler, J., Helbig, M., Kühn, K., Bachmann, T., Hartsch, J., and Henker, J., 2011, Zinnwald Lithium Project.

Neßler, J., Seifert, T., Gutzmer, J., Müller, A., Henker, J., and Kühn, K., New lithogeochemical and mineralogical exploration of Li-Sn greisen mineralisation in old mining adits of the Zinnwald deposit, Germany, *in* Proceedings EGU General Assembly Conference Abstracts2014, Volume 16.

Plessen, B., and Lüders, V., 2012, Simultaneous measurements of gas isotopic compositions of fluid inclusion gases (N2, CH4, CO2) using continuous-flow isotope ratio mass spectrometry: Rapid Communications in Mass Spectrometry, v. 26, no. 9, p. 1157-1161.

Roedder, E., 1984, Fluid inclusions, Mineralogical Society of America Reviews in Mineralogy Volume 12.

Romer, R., and Kroner, U., 2015, Sediment and weathering control on the distribution of Paleozoic magmatic tin–tungsten mineralization: Mineralium Deposita, v. 50, p. 327-338.

Romer, R. L., and Kroner, U., 2016, Phanerozoic tin and tungsten mineralization—Tectonic controls on the distribution of enriched protoliths and heat sources for crustal melting: Gondwana Research, v. 31, p. 60-95.

Rub, A. K., Štemprok, M., and Rub, M. G., 1998, Tantalum mineralization in the apical part of the Cínovec (Zinnwald) granite stock: Mineralogy and Petrology, v. 63, p. 199-222.

Schlöglova, K., Wälle, M., and Heinrich, C. A., 2017, LA-ICP-MS analysis of fluid inclusions: contamination effects challenging micro-analysis of elements close to their detection limit: J. Anal. At. Spectrom., v. 32, no. 5, p. 1052-1063.

Sebastian, U., 2013, Die Geologie des Erzgebirges, Springer Spektrum, 268 p.:

Seifert, T., Atanasove, P., Gutzmer, J., and Pfänder, J., 2011, Mineralogy, geochemistry and age of greisen mineralization in the Li–Rb–Cs–Sn–W deposit Zinnwald, Erzgebirge, Germany: Mineral Mag, v. 75, no. Suppl, p. 1833.

Seltmann, R., 1994, Sub-volcanic minor intrusions in the Altenberg Caldera and their Metallogeny, *in* Seltmann, R., Kämpf, H., and Möller, P., eds., Metallogeny of collisional Orogens: Prague, Czech Geological Survey.

Štemprok, M., Dolejš, D., and Holub, F. V., 2014, Late Variscan calc-alkaline lamprophyres in the Krupka ore district, Eastern Krušné hory/Erzgebirge: their relationship to Sn-W mineralization: Journal of Geosciences, v. 59, p. 41-68.

Štemprok, M., 1965, Petrology and the vertical extent of mineralization in the Cínovec (Zinnwald) granite cupola: Sbor. Geol. Věd, v. LG 5, p. 7-106.

-, 1971, Petrochemical features of tin-bearing granites in the Krušné Hory Mts., Czechoslovakia: Soc. Mining Geol. Japan, Special issue, v. 2, p. 112-118.

Štemprok, M., Novák, J. K., and David, J., 1994, The association between granites and tin-tungsten mineralization in the eastern Krušné hory (Erzgebirge), Czech Republic: Monograph Series on Mineral Deposits, v. 31, p. 97-129.

Štemprok, M., and Sulcek, Z., 1969, Geochemical profile through an ore- bearing Lithium Granite: Economic Geology, v. 64, p. 392-404.

Thomas, R., 1982, Ergebnisse der thermobarogeochemischen Untersuchungen an Flüssigkeitseinschlüssen in Mineralen der postmagmatischen Zinn-Wolfram-Mineralisation des Erzgebirges: Freiberger Forschungsheft R. C, v. C 370, p. 1-85.

Thomas, R., and Baumann, L., 1980, Ergebnisse von thermometrischen und kryometrischen Untersuchungen an Kassiteriten des Erzgebirges: Zeitschrift für geologische Wissenschaften, Berlin, v. 10, p. 1281-1299.

Webster, J., Thomas, R., Förster, H.-J., Seltmann, R., and Tappen, C., 2004, Geochemical evolution of halogen-enriched granite magmas and mineralizing fluids of the Zinnwald tin-tungsten mining district, Erzgebirge, Germany: Mineralium Deposita, v. 39, no. 4, p. 452-472.